LOW-THRUST COLLISION AVOIDANCE DESIGN FOR LEO MISSIONS WITH RETURN TO NOMINAL ORBIT

Andrea De Vittori[*], Gabriele Dani[†], Pierluigi Di Lizia[‡], and Roberto Armellin [§]

This work investigates the design of optimal and computationally efficient low-thrust Collision Avoidance Maneuvers (CAMs) in the LEO regime. A potential collision is prevented thanks to two different CAM policies. The first one enforces a certain threshold on the Probability of Collision (PoC) at the Time of Closest Approach (TCA); then, the spacecraft targets a point belonging to its nominal orbit. For this purpose, the conjunction dynamics of the two objects are presented in a Cartesian reference system and then projected onto the B-plane, centred on the secondary object. The second method forces the satellite to match the original Keplerian parameters, leaving out the true anomaly.

INTRODUCTION

The number of artificial objects around the Earth, no longer functional for operative applications, has gradually built up in the form of high-speed clutter that is on the verge of jeopardizing the future of space activity. Among all orbital regimes, LEO is the most congested region for remote sensing, imaging, and commercial applications due to its close proximity to the Earth. The intensive usage has transformed it into a bullet depository with an unabated proliferation of rocket bodies, paint flecks, mission-related payloads, and fragments from previous collisions. In 2009, the European Space Agency (ESA) started the Space Situational Awareness (SSA) Program to let Europe acquire the independent capability to watch and monitor objects and natural phenomena that could harm both on-ground and on-orbit facilities (for further information check[1]). To avoid a cascading effect, one of the provided services is preventing in-space impacts through a careful choice of orbits placement and by performing Collision Avoidance Maneuvers (CAMs). Within this framework, once satellite controllers receive an alert, they wisely design CAMs targeting a safeguard limit for a target Probability of Collision (PoC) that does not affect fuel consumption too much. Current CAM routines are specifically conceived for impulsive propulsion systems present in the vast majority of orbiting assets. With the rise of low-thrust technology, bespoke CAM policies should optimally decide when to switch on the engine to act safely in close encounters. Furthermore, CAMs decision-making has to progressively migrate from on-ground planning to an onboard implementation to alleviate the workload on operators owing to an ever-growing number of active

[*]Phd candidate, Department of Aerospace Science and Technology, Politecnico di Milano via Privata Giuseppe La Masa 34, Milano, 20156. Email: andrea.devittori@polimi.it

[†]Graduate student, Department of Aerospace Engineering, Politecnico di Milano, Via Privata Giuseppe La Masa 34, Milano, Lombardia, Italia 20156. Email: gabiele.dani@mail.polimi.it

[‡]Associate professor, Department of Aerospace Science and Technology, Politecnico di Milano via Privata Giuseppe La Masa 34, Milano, 20156. Email: pierluigi.dilizia@polimi.it

[§]Professor, Department of Aerospace Engineering, University of Auckland, 20 Symonds Street, Auckland Central, Auckland, New Zealand 1010. Email: roberto.armellin@auckland.ac.nz

satellites. Given the limited computational power, satellites should lean on lightweight algorithms to make all this possible. Another vitally important aspect is commanding a post-CAM maneuver to ease the spacecraft reenter to its nominal orbit.
The literature regarding the optimization of impulsive collision avoidance practices is the most thorough; however, over the last years, researchers have deepened the theory behind low-thrust CAMs. Studies on low-thrust optimization methods include the semi-analytical method developed by Reiter et al.[2] for rapid collision avoidance, supposing an optimal radial thrust, but it is valid just in proximity of conjunction. In 2022, De Vittori[3] excogitated an analytic solution for the energy-optimal CAM imposing PoC at TCA as the terminal constraint, in cartesian coordinates and B-plane dynamics formulation. The EOCP policy serves as a first-attempt solution for a Fuel Optimal CAM shaped by a bang-bang acceleration at the expense of a time-consuming algorithm. More semi-analytical methods were proposed in;[4] this approach harnesses average dynamics maximizing the miss distance with the assumption of continuous tangential thrust. Bombardelli and Hernando-Ayuso[5] investigated the problem of optimum low-thrust collision avoidance between two objects in circular orbits; the thrust vector of the maneuvered satellite, applied continuously for a given time span, is held constant in magnitude and only the orientation can be adjusted. The optimal control is written in B-plane coordinates to lessen the dimension of the resulting Two Boundary Point value Problem (2PBVP) to only two with a constant costate vector. Martinez Chamarro et al.[6] present two ways to compute low-thrust CAMs; the first approximates a bang-bang structure by applying a smoothing approach to an EOP continuous solution. In the second method, the maneuver design derives from a convex optimization problem. In 2012, Lee developed a collision avoidance maneuver for LEO and Geostationary Earth Orbit (GEO) satellites maintained in a keeping area.[7] GA-based optimization scheme gets both the maneuver start time and the Δv to reduce collision likelihood with uncontrolled space objects or debris. The limitation of GA resides in the numerical effort.
The state-of-art CAM optimization does not cover the reentry to the nominal orbit in the overall maneuver decision-making. In this context, the work initially addresses CAM in LEO as an (EOCP) leveraging a Three-Point Boundary Value Problem (3PBVP) formulation stemming from[8] for embedded CAM and SK in GEO. The underlying idea is to devise a CAM that either fixes the terminal state or a set of keplerian elements, leaving free the final true anomaly, after TCA through motion linearization.

FUNDAMENTALS

This section defines the theoretical knowledge needed for the analytical CAM formulation.

Conjunction definition

The CAM design process starts evaluating the short-term encounter between a satellite and debris. The controllable object (called primary object) is described by a state $\mathbf{x}_p = [\mathbf{r}_p; \mathbf{v}_p]$ while debris (secondary object) is identified by the state $\mathbf{x}_s = [\mathbf{r}_s; \mathbf{v}_s]$. In this equations, $\mathbf{r}_i$ and $\mathbf{v}_i$ are the position and the velocity of the centre of mass of the single object measured in a generic reference $\hat{\Re}$. To compute the collision probability, a useful coordinate system is the B-Plane. The origin of this frame lies at the centre of the secondary object at the time of closest approach as depicted in Fig. 1, with the following axes direction:

$$\mathbf{u}_\xi = \frac{\mathbf{v}_p \times \mathbf{v}_s}{||\mathbf{v}_p \times \mathbf{v}_s||},\ \mathbf{u}_\eta = \frac{\mathbf{v}_p - \mathbf{v}_s}{||\mathbf{v}_p - \mathbf{v}_s||},\ \mathbf{u}_\zeta = \mathbf{u}_\xi \times \mathbf{u}_\eta \tag{1}$$

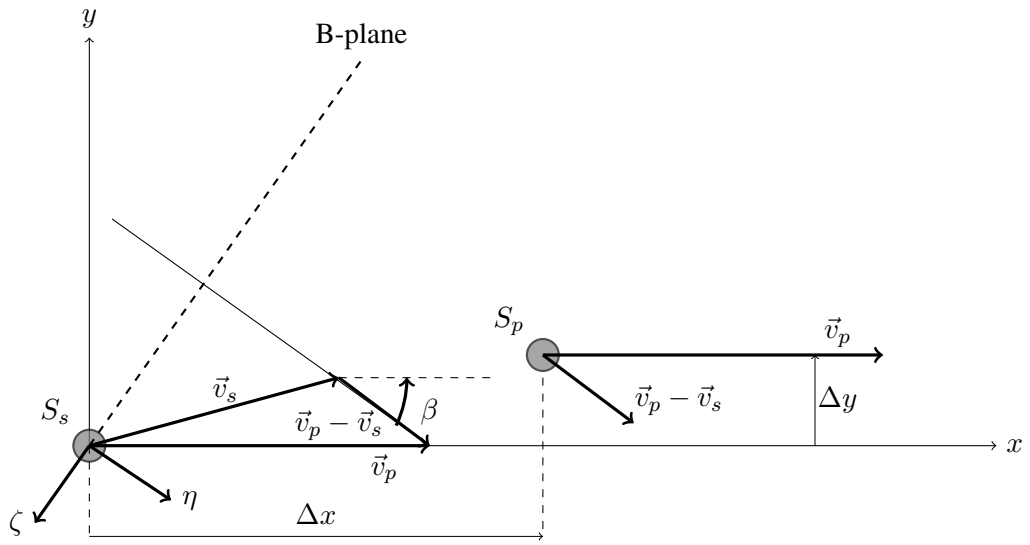

Figure 1: BPlane representation[9]

Consequently, the position vector in the B-Plane reference frame is identified as $\mathbf{b}_{3D} = [\xi, \eta, \zeta]^\top$. The rotation matrix to pass from the inertial reference to the B-Plane one is defined as:

$$\mathbf{R}_{b,3D} = [\mathbf{u}_\xi, \mathbf{u}_\eta, \mathbf{u}_\zeta]^\top \tag{2}$$

Additionally, the projection on the η axis is given by:

$$\mathbf{R}_{b,2D} = [\mathbf{u}_\xi, \mathbf{u}_\zeta]^\top \tag{3}$$

Consequently, the 2D position vector in the B-Plane is defined as $\mathbf{b} = [\xi, \zeta]^\top$.

Chan's PoC model

PoC between the primary and secondary objects experiencing a short-term conjunction can be obtained by integrating the relative position probability density function over a sphere of radius R_A (i.e. the hard body sphere given by the summed primary and secondary radii) at TCA. This assumption is made up for the lack of information about attitude and geometry, especially for the secondary object.[10] Assuming that the relative probability distribution function is Gaussian, an approximated collision probability is obtained with the Chan's method of equivalent cross-sectional areas:

$$\mathrm{PoC}(u, v) = e^{-\frac{v}{2}} \sum_{m=0}^{\infty} \frac{v^m}{2^m m!} \left[1 - e^{-\frac{u}{2}} \sum_{k=0}^{m} \frac{u^k}{2^k k!} \right] \tag{4}$$

Where u is the ratio of the impact cross-sectional area to the 1σ B-Plane covariance ellipse area:

$$u = \frac{s_A^2}{\sigma_\xi \sigma_\zeta \sqrt{1 - \rho_{\xi\zeta}^2}} \tag{5}$$

and v is the Squared Mahalanobis Distance (SMD):

$$\begin{aligned} v &= (\mathbf{r}_p - \mathbf{r}_s)^\top \mathbf{R}_{b,2D}^\top \mathbf{C}^{-1} \mathbf{R}_{b,2D} (\mathbf{r}_p - \mathbf{r}_s) = \\ &= \mathbf{b}_p^\top \mathbf{C}^{-1} \mathbf{b}_p \end{aligned} \tag{6}$$

where: $\mathbf{C}$ is the covariance matrix, and $\mathbf{b}_p$ is the primary object position relative to the secondary object in the B-Plane framework.

State Transition Matrix

Given the non-linear dynamics described in the previous section, the STM labelled as $\mathbf{\Phi}$ allows to map an arbitrary state variation at a certain time t_0 to a final one at t_f according to the following equation:

$$\delta\mathbf{x}_f = \mathbf{\Phi}\delta\mathbf{x}_0 \tag{7}$$

For time-varying systems, $\mathbf{\Phi}(t, t_0)$ can be found by integrating the following equation:

$$\dot{\mathbf{\Phi}}(t, t_0) = \mathbf{A}(t)\mathbf{\Phi}(t, t_0),\ \mathbf{\Phi}(t_0, t_0) = \mathbf{I} \tag{8}$$

where $\mathbf{\Phi}(t_0, t_0)$ is the initial condition and $\mathbf{A}(t)$ is the state matrix obtained by means of a linearization of the dynamical system $\boldsymbol{f}(\mathbf{x}, t)$ around the nominal trajectory $\mathbf{x}_n$:

$$\mathbf{A} = \left.\frac{\partial \boldsymbol{f}(\mathbf{x}, t)}{\partial \mathbf{x}}\right|_{\mathbf{x}_n} \tag{9}$$

ENERGY-OPTIMAL LEO CAM DESIGN

The LEO design comprises two control strategies. The Point to Point (PTP) in ECI formalism fixes the final state over the nominal trajectory after CAM for a specified time. The Point to Orbit (PTO) lets the EOCP choose the optimal reentry point by targeting just five of the six orbital elements.

Point-to-Point with intermediate CAM constraint

The main objective of CAMs is to minimize both PoC and propellant consumption through the definition of a cost function J:

$$J := \nu\Psi(t_{ca}, \mathbf{x}(t_{ca})) + \int_{t_0}^{t_f} \frac{1}{2}{\mathbf{a_c}}^T\mathbf{a_c}dt \tag{10}$$

Where:

$$\Psi(t_{ca}, \mathbf{x}(t_{ca})) = SMD(\mathbf{r}(t_{ca})) - \overline{SMD} = 0 \tag{11}$$

Ψ represents the interior point equality constraint on the SMD at the time of the closest approach (t_{ca}). Thanks to Pontryiagin's maximum principle, the optimal control solution results from the

following Multi-Point Boundary Value Problem (MPBVP) set in Keplerian dynamics:

$$\begin{cases} \dot{\mathbf{r}} = \mathbf{v} \\ \dot{\mathbf{v}} = -\dfrac{mu}{r^3}\mathbf{r} - \boldsymbol{\lambda_v} \\ \dot{\boldsymbol{\lambda}}_{\boldsymbol{r}} = \dfrac{\mu}{r^3}\boldsymbol{\lambda_v} - \dfrac{3\mu \mathbf{r}^T \boldsymbol{\lambda_v}}{r^5}\mathbf{r} \\ \dot{\boldsymbol{\lambda}}_{\boldsymbol{v}} = -\boldsymbol{\lambda_r} \end{cases}$$
$$\begin{cases} \mathbf{x}(t_0) = \mathbf{x_0} \\ \mathbf{x}(t_{ca^-}) = \mathbf{x}(t_{ca^+}) \\ \nu \dfrac{\partial \Psi}{\partial \mathbf{x}(t_{ca})} - \boldsymbol{\lambda}^T(t_{ca}^-) + \boldsymbol{\lambda}^T(t_{ca}^+) = 0 \\ \mathbf{x}(t_f) = \mathbf{x_f} \\ \Psi(t_{ca}) = 0 \end{cases} \tag{12}$$

The problem turns into finding the initial costate $\boldsymbol{\lambda_0}$ and the adjoined multiplier ν. $\mathbf{x_f}$ is the state on the ballistic orbit at t_f. The solution scheme subdivides the trajectory into two intervals $[t_1; t_{ca}]$ and $[t_{ca}; t_f]$ because the interior point constraint applies at TCA. For an analytical solution, the two trajectories are linearized with respect to the Keplerian unperturbed motion by virtue of the STM.

$$\begin{cases} \dot{\boldsymbol{\Phi}}(t) = \mathbf{A}(t)\boldsymbol{\Phi}(\mathbf{x}(t_0), t) \\ \boldsymbol{\Phi}(\mathbf{x}(t_0), t_0) = \mathbf{I} \end{cases} \tag{13}$$

Where:

$$\mathbf{A} = \begin{bmatrix} \mathbf{0_{3\times3}} & \mathbf{I_{3\times3}} & \mathbf{0_{3\times3}} & \mathbf{0_{3\times3}} \\ \frac{3\mu}{r^5}\mathbf{r}\mathbf{r}^T - \frac{\mu}{r^3}\mathbf{I_{3\times3}} & \mathbf{0_{3\times3}} & \mathbf{0_{3\times3}} & -\mathbf{I_{3\times3}} \\ \mathbf{0_{3\times3}} & \mathbf{0_{3\times3}} & \mathbf{0_{3\times3}} & \frac{\mu}{r^3}\mathbf{I_{3\times3}} - \frac{3\mu}{r^5}\mathbf{r}\mathbf{r}^T \\ \mathbf{0_{3\times3}} & \mathbf{0_{3\times3}} & -\mathbf{I_{3\times3}} & \mathbf{0_{3\times3}} \end{bmatrix}$$

The linearization of the first arc brings to the following system of equations:

$$\begin{bmatrix} \boldsymbol{\delta}\mathbf{r_{ca}} \\ \boldsymbol{\delta}\mathbf{v_{ca}} \\ \boldsymbol{\delta\lambda}_{\boldsymbol{r_{ca}}}^- \\ \boldsymbol{\delta\lambda}_{\boldsymbol{v_{ca}}}^- \end{bmatrix} = \begin{bmatrix} \boldsymbol{\Phi_{11}} & \boldsymbol{\Phi_{12}} & \boldsymbol{\Phi_{13}} & \boldsymbol{\Phi_{14}} \\ \boldsymbol{\Phi_{21}} & \boldsymbol{\Phi_{22}} & \boldsymbol{\Phi_{23}} & \boldsymbol{\Phi_{24}} \\ \boldsymbol{\Phi_{31}} & \boldsymbol{\Phi_{32}} & \boldsymbol{\Phi_{33}} & \boldsymbol{\Phi_{34}} \\ \boldsymbol{\Phi_{41}} & \boldsymbol{\Phi_{42}} & \boldsymbol{\Phi_{43}} & \boldsymbol{\Phi_{44}} \end{bmatrix} \begin{bmatrix} \boldsymbol{\delta}\mathbf{r_0} \\ \boldsymbol{\delta}\mathbf{v_0} \\ \boldsymbol{\delta\lambda}_{r_0} \\ \boldsymbol{\delta\lambda}_{v_0} \end{bmatrix} \tag{14}$$

Rearranging the first two rows, starting from the initial conditions $\boldsymbol{\delta}\mathbf{r_0} = \boldsymbol{\delta}\mathbf{v_0} = \mathbf{0}$, the initial co-state expresses as a function of the perturbation of the state at TCA.

$$\begin{cases} \boldsymbol{\delta\lambda}_{r_0} = \mathbf{D}\boldsymbol{\delta}\mathbf{r_{ca}} + \mathbf{E}\boldsymbol{\delta}\mathbf{v_{ca}} \\ \boldsymbol{\delta\lambda}_{v_0} = \mathbf{M}\boldsymbol{\delta}\mathbf{r_{ca}} + \mathbf{B}\boldsymbol{\delta}\mathbf{v_{ca}} \end{cases} \tag{15a}$$

$$\mathbf{M} = -\mathbf{B}\boldsymbol{\Phi_{23}}\boldsymbol{\Phi_{13}}^{-1} \qquad \mathbf{B} = [\boldsymbol{\Phi_{24}} - \boldsymbol{\Phi_{23}}\boldsymbol{\Phi_{13}}^{-1}\boldsymbol{\Phi_{14}}]^{-1} \tag{15b}$$

$$\mathbf{D} = [\boldsymbol{\Phi_{13}}^{-1} - \boldsymbol{\Phi_{13}}^{-1}\boldsymbol{\Phi_{14}}\mathbf{M}] \qquad \mathbf{E} = -\boldsymbol{\Phi_{13}}^{-1}\boldsymbol{\Phi_{14}}\mathbf{B} \tag{15c}$$

The symbol δ for the co-state variables is redundant because the variation is null along the un-maneuvered trajectory. Consequently, this symbol is now on omitted for conciseness.

Eqs. 15a come in handy to make the costates at TCA- dependent on the state at conjunction:

$$\begin{cases} \boldsymbol{\lambda}_{r_{ca}}^{-} = [\mathbf{\Phi_{33}D} + \mathbf{\Phi_{34}M}]\boldsymbol{\delta}\mathbf{r_{ca}} + [\mathbf{\Phi_{34}B} + \mathbf{\Phi_{33}E}]\boldsymbol{\delta}\mathbf{v_{ca}} \\ \boldsymbol{\lambda}_{v_{ca}}^{-} = [\mathbf{\Phi_{43}D} + \mathbf{\Phi_{44}M}]\boldsymbol{\delta}\mathbf{r_{ca}} + [\mathbf{\Phi_{44}B} + \mathbf{\Phi_{43}E}]\boldsymbol{\delta}\mathbf{v_{ca}} \end{cases} \Longrightarrow \begin{cases} \boldsymbol{\lambda}_{r_{ca}}^{-} = \mathbf{F}\boldsymbol{\delta}\mathbf{r_{ca}} + \mathbf{G}\boldsymbol{\delta}\mathbf{v_{ca}} \\ \boldsymbol{\lambda}_{v_{ca}}^{-} = \mathbf{H}\boldsymbol{\delta}\mathbf{r_{ca}} + \mathbf{L}\boldsymbol{\delta}\mathbf{v_{ca}} \end{cases} \tag{16a}$$

$$\mathbf{F} = [\mathbf{\Phi_{33}D} + \mathbf{\Phi_{34}M}] \qquad \mathbf{G} = [\mathbf{\Phi_{34}B} + \mathbf{\Phi_{33}E}] \tag{16b}$$

$$\mathbf{H} = [\mathbf{\Phi_{43}D} + \mathbf{\Phi_{44}M}] \qquad \mathbf{L} = [\mathbf{\Phi_{44}B} + \mathbf{\Phi_{43}E}] \tag{16c}$$

For the secondary arc, the state variables and the velocity co-state are continuous at TCA; the interior point constraint imposes a discontinuity on the position co-state. The final target point lies in the un-maneuvered Keplerian orbit. For this reason, the perturbation of the final state needs to be assumed as $\boldsymbol{\delta}\mathbf{r_f} = \boldsymbol{\delta}\mathbf{v_f} = \mathbf{0}$

$$\begin{bmatrix} \boldsymbol{\delta}\mathbf{r_f} \\ \boldsymbol{\delta}\mathbf{v_f} \\ \boldsymbol{\lambda}_{r_f} \\ \boldsymbol{\lambda}_{v_f} \end{bmatrix} = \begin{bmatrix} \tilde{\mathbf{\Phi}}_{\mathbf{11}} & \tilde{\mathbf{\Phi}}_{\mathbf{12}} & \tilde{\mathbf{\Phi}}_{\mathbf{13}} & \tilde{\mathbf{\Phi}}_{\mathbf{14}} \\ \tilde{\mathbf{\Phi}}_{\mathbf{21}} & \tilde{\mathbf{\Phi}}_{\mathbf{22}} & \tilde{\mathbf{\Phi}}_{\mathbf{23}} & \tilde{\mathbf{\Phi}}_{\mathbf{24}} \\ \tilde{\mathbf{\Phi}}_{\mathbf{31}} & \tilde{\mathbf{\Phi}}_{\mathbf{32}} & \tilde{\mathbf{\Phi}}_{\mathbf{33}} & \tilde{\mathbf{\Phi}}_{\mathbf{34}} \\ \tilde{\mathbf{\Phi}}_{\mathbf{41}} & \tilde{\mathbf{\Phi}}_{\mathbf{42}} & \tilde{\mathbf{\Phi}}_{\mathbf{43}} & \tilde{\mathbf{\Phi}}_{\mathbf{44}} \end{bmatrix} \begin{bmatrix} \boldsymbol{\delta}\mathbf{r_{ca}} \\ \boldsymbol{\delta}\mathbf{v_{ca}} \\ \boldsymbol{\lambda}_{r_{ca}}^{+} \\ \boldsymbol{\lambda}_{v_{ca}}^{+} \end{bmatrix} \tag{17}$$

Recalling the co-state discontinuity expressed in the boundary conditions of Eq. 12, and substituting the expression of the SMD constraint derivative:

$$\begin{cases} \boldsymbol{\lambda}_{r_{ca}}^{+} = \boldsymbol{\lambda}_{r_{ca}}^{-} - 2\nu {\mathbf{R_{2b}}}^{T}\mathbf{C}^{-1}\mathbf{R_{2b}}\boldsymbol{\delta}\mathbf{r_{imp}^{m}} \\ \boldsymbol{\lambda}_{v_{ca}}^{+} = \boldsymbol{\lambda}_{v_{ca}}^{-} \end{cases} \tag{18}$$

Where $\boldsymbol{\delta}\mathbf{r_{imp}^{m}} = \mathbf{r_{ca}^{m}} - \mathbf{r_s}$ is the position vector from the secondary object at TCA to the primary in cartesian coordinates.

Working on the first two vectorial equations of system 17 and substituting Eq. 16a and Eq. 18 it reads:

$$\tilde{\mathbf{N}}\boldsymbol{\delta}\mathbf{r_{ca}} + \tilde{\mathbf{P}}\boldsymbol{\delta}\mathbf{v_{ca}} - \nu\tilde{\mathbf{Q}}\mathbf{R_{2b}}\boldsymbol{\delta}\mathbf{r_{imp}^{m}} = \mathbf{0} \tag{19a}$$

$$\begin{aligned} \tilde{\mathbf{N}} &= [\tilde{\mathbf{\Phi}}_{\mathbf{11}} + \tilde{\mathbf{\Phi}}_{\mathbf{14}}\mathbf{H} + \tilde{\mathbf{\Phi}}_{\mathbf{13}}\mathbf{F}] \\ \tilde{\mathbf{P}} &= [\tilde{\mathbf{\Phi}}_{\mathbf{12}} + \tilde{\mathbf{\Phi}}_{\mathbf{14}}\mathbf{L} + \tilde{\mathbf{\Phi}}_{\mathbf{13}}\mathbf{G}] \\ \tilde{\mathbf{Q}} &= 2\tilde{\mathbf{\Phi}}_{\mathbf{13}}{\mathbf{R_{2b}}}^{T}\mathbf{C}^{-1} \end{aligned} \tag{19b}$$

And:

$$\mathbf{N}\boldsymbol{\delta}\mathbf{r_{ca}} + \mathbf{P}\boldsymbol{\delta}\mathbf{v_{ca}} - \nu\mathbf{Q}\mathbf{R_{2b}}\boldsymbol{\delta}\mathbf{r_{imp}^{m}} = \mathbf{0} \tag{20a}$$

$$\begin{aligned} \mathbf{N} &= [\tilde{\mathbf{\Phi}}_{\mathbf{21}} + \tilde{\mathbf{\Phi}}_{\mathbf{24}}\mathbf{H} + \tilde{\mathbf{\Phi}}_{\mathbf{23}}\mathbf{F}]; \\ \mathbf{P} &= [\tilde{\mathbf{\Phi}}_{\mathbf{22}} + \tilde{\mathbf{\Phi}}_{\mathbf{24}}\mathbf{L} + \tilde{\mathbf{\Phi}}_{\mathbf{23}}\mathbf{G}]; \\ \mathbf{Q} &= 2\tilde{\mathbf{\Phi}}_{\mathbf{23}}{\mathbf{R_{2b}}}^{T}\mathbf{C}^{-1} \end{aligned} \tag{20b}$$

Eq. 20a can be solved for $\boldsymbol{\delta \mathbf{v}_{\mathbf{ca}}}$ and substituted in Eq. 19 in order to find the expression of $\boldsymbol{\delta \mathbf{r}_{\mathbf{ca}}}$ as a function of the position vector $\boldsymbol{\delta \mathbf{r}^{\mathbf{m}}_{\mathbf{imp}}}$ and the multiplier ν:

$$\boldsymbol{\delta \mathbf{r}_{\mathbf{ca}}} = \nu \mathbf{S}^{-1} \mathbf{T} \mathbf{R}_{\mathbf{2b}} \boldsymbol{\delta \mathbf{r}^{\mathbf{m}}_{\mathbf{imp}}} \tag{21a}$$

$$\mathbf{S} = [\tilde{\mathbf{N}} - \tilde{\mathbf{P}} \mathbf{P}^{-1} \mathbf{N}] \qquad \mathbf{T} = [\tilde{\mathbf{Q}} - \tilde{\mathbf{P}} \mathbf{P}^{-1} \mathbf{Q}] \tag{21b}$$

The last step is combining the preceding relations with the SMD constraint at TCA. This can be done by adding and subtracting $\mathbf{r_s}$ on the left term and then premultiplying Eq. 21a by $\mathbf{R_{2b}}$. This operation transfers the problem to B-plane.

$$\mathbf{R_{2b}} [\mathbf{r^m_{ca}} - \mathbf{r_s} - \mathbf{r_{ca}} + \mathbf{r_s}] = \nu \mathbf{R_{2b}} \mathbf{S}^{-1} \mathbf{T} \mathbf{R_{2b}} \boldsymbol{\delta \mathbf{r}^{\mathbf{m}}_{\mathbf{imp}}} \tag{22a}$$

$$\mathbf{R_{2b}} [\boldsymbol{\delta \mathbf{r}^{\mathbf{m}}_{\mathbf{imp}}} - \boldsymbol{\delta \mathbf{r}_{\mathbf{imp}}}] = \nu \mathbf{R_{2b}} \mathbf{S}^{-1} \mathbf{T} \mathbf{R_{2b}} \boldsymbol{\delta \mathbf{r}^{\mathbf{m}}_{\mathbf{imp}}} \tag{22b}$$

$$\mathbf{b^m_{imp}} - \mathbf{b_{imp}} = \nu \mathbf{R_{2b}} \mathbf{S}^{-1} \mathbf{T} \mathbf{b^m_{imp}} \tag{22c}$$

The previous equation can be inverted to retrieve an expression just function of the un-maneuvered position vector in B-plane.

$$\mathbf{b^m_{imp}} = [\mathbf{I} - \nu \mathbf{U}]^{-1} \mathbf{b_{imp}} \tag{23a}$$

$$\mathbf{U} = \mathbf{R_{2b}} \mathbf{S}^{-1} \mathbf{T} \tag{23b}$$

Finally, with the following linear algebra relation:

$$[\mathbf{I} - \nu \mathbf{U}]^{-1} = \frac{1}{det(\mathbf{I} - \nu \mathbf{U})} [\mathbf{I} - \nu det(\mathbf{U}) \mathbf{U}^{-1}] \tag{24}$$

And applying the constraint on the SMD, a fourth-degree-equation solves analytically with unknown ν:

$$\begin{gathered} \nu^2 \mathbf{b_{imp}}^T \mathbf{Z}^T \mathbf{C}^{-1} \mathbf{Z} \mathbf{b_{imp}} - \nu \mathbf{b_{imp}}^T [\mathbf{Z}^T \mathbf{C}^{-1} + \mathbf{C}^{-1} \mathbf{Z}] \mathbf{b_{imp}} = \\ \alpha^2 \overline{SMD} - \mathbf{b_{imp}}^T \mathbf{C}^{-1} \mathbf{b_{imp}} \end{gathered} \tag{25a}$$

$$\alpha = det(\mathbf{I} - \nu \mathbf{U}) \qquad \mathbf{Z} = det(\mathbf{U}) \mathbf{U}^{-1} \tag{25b}$$

Among the four solutions of Eq. 25a there are two real local minima and two local maxima (depending on the polynomial coefficients) in terms of equivalent Δv. Once the value of ν is known, the initial costates come straight forward by following backwards the algorithm.

Point-to-Orbit with intermediate CAM constraint

The objective is to minimize the following functional:

$$J := \nu \Pi(t_{ca}, \mathbf{x}(t_{ca})) + \int_{t_i}^{t_f} \frac{1}{2} \mathbf{a_c}^T \mathbf{a_c} dt \tag{26}$$

where Π represents again the interior point equality constraint on the SMD.
The main difference compared to the previous method lies in the terminal constraints. In fact, to fix

the orbit reentry, one sets five orbital elements leaving free the final true anomaly.
Pontryagin's maximum principle leads to the definition of the following Three Point BVP:

$$\begin{cases} \dot{\mathbf{x}} = \mathbf{f}(\mathbf{x}, \mathbf{a_c}) \\ \dot{\boldsymbol{\lambda}} = -\left[\dfrac{\partial \mathbf{f}}{\partial \mathbf{x}}\right]^T \boldsymbol{\lambda} \end{cases}$$
$$\begin{cases} \mathbf{x}(t_0) = \mathbf{x_0} \\ \mathbf{x}(t_{ca^-}) = \mathbf{x}(t_{ca^+}) \\ \nu \dfrac{\partial \Pi}{\partial \mathbf{x}(t_{ca})} - \boldsymbol{\lambda}^T(t_{ca}^-) + \boldsymbol{\lambda}^T(t_{ca}^+) = 0 \\ \mathbf{x}'(t_f) = \mathbf{x}'_\mathbf{f} \\ \boldsymbol{\lambda_\theta}(t_f) = 0 \\ \Pi(t_{ca}) = 0 \end{cases}, \; where: \mathbf{x}' = \begin{bmatrix} a \\ e \\ i \\ \Omega \\ \omega \end{bmatrix} \tag{27}$$

Similarly to the previous derivation, the problem comes down to computing the initial co-state and the multiplier ν. The objective is to find the expression of the co-state at TCA as a function of the state perturbation at the same instant:

$$\begin{bmatrix} \boldsymbol{\delta}\mathbf{x_{ca^-}} \\ \boldsymbol{\lambda_{ca^-}} \end{bmatrix} = \begin{bmatrix} \boldsymbol{\Phi_{xx}} & \boldsymbol{\Phi_{x\lambda}} \\ \boldsymbol{\Phi_{\lambda x}} & \boldsymbol{\Phi_{\lambda\lambda}} \end{bmatrix} \begin{bmatrix} \boldsymbol{\delta}\mathbf{x_0} \\ \boldsymbol{\lambda_0} \end{bmatrix} \tag{28a}$$

$$\boldsymbol{\lambda_{ca^-}} = \boldsymbol{\Phi_{\lambda\lambda}} \boldsymbol{\Phi_{x\lambda}}^{-1} \boldsymbol{\delta}\mathbf{x_{ca^-}} \tag{28b}$$

In view of the second part, it will be useful decompose Eq. 28b as done with the state vector in Eq. 27:

$$\boldsymbol{\lambda'_{ca^-}} = \mathbf{E}\boldsymbol{\delta}\mathbf{x'_{ca^-}} + \mathbf{w}\theta_{ca^-} \tag{29a}$$

$$\lambda_{\theta_{ca^-}} = \mathbf{g}\boldsymbol{\delta}\mathbf{x'_{ca^-}} + P\theta_{ca^-} \tag{29b}$$

Where:

$$\boldsymbol{\lambda'} = \begin{bmatrix} \lambda_a \\ \lambda_e \\ \lambda_i \\ \lambda_\Omega \\ \lambda_\omega \end{bmatrix} \qquad \boldsymbol{\Phi_{\lambda\lambda}} \boldsymbol{\Phi_{x\lambda}}^{-1} = \begin{bmatrix} \mathbf{E} & \mathbf{w} \\ \mathbf{g} & P \end{bmatrix} \tag{30}$$

For this particular problem, the analytic solution needs to introduce a zero-order Taylor expansion linked to the co-state discontinuity equation.

$$\frac{\partial \Pi}{\partial \mathbf{x}(t_{ca})} = \boldsymbol{\varphi}(\mathbf{x_{ca}}) \approx \boldsymbol{\varphi}(\mathbf{x_{ref}}(t_{ca})) = \boldsymbol{\varphi} \tag{31}$$

The discontinuity equation can be split as:

$$\begin{aligned} \boldsymbol{\lambda'_{ca^+}} &= \boldsymbol{\lambda'_{ca^-}} - \nu\boldsymbol{\varphi'} \\ \lambda_{\theta_{ca^+}} &= \lambda_{\theta_{ca^-}} - \nu\varphi_\theta \end{aligned} \tag{32}$$

The previous decomposition of the first five orbital elements and the last co-state variable is crucial for the terminal boundary conditions.

$$\begin{bmatrix} \boldsymbol{\delta \mathbf{x}'_{\mathbf{f}}} \\ \delta\theta_f \\ \boldsymbol{\lambda'_f} \\ \lambda_{\theta_f} \end{bmatrix} = \begin{bmatrix} \tilde{\boldsymbol{\Phi}}_{\boldsymbol{x'x'}} & \tilde{\boldsymbol{\Phi}}_{\boldsymbol{x'\theta}} & \tilde{\boldsymbol{\Phi}}_{\boldsymbol{x'\lambda'}} & \tilde{\boldsymbol{\Phi}}_{\boldsymbol{x'\lambda_\theta}} \\ \tilde{\boldsymbol{\Phi}}_{\boldsymbol{\theta x'}} & \tilde{\boldsymbol{\Phi}}_{\boldsymbol{\theta\theta}} & \tilde{\boldsymbol{\Phi}}_{\boldsymbol{\theta\lambda'}} & \tilde{\boldsymbol{\Phi}}_{\boldsymbol{\theta\lambda_\theta}} \\ \tilde{\boldsymbol{\Phi}}_{\boldsymbol{\lambda' x'}} & \tilde{\boldsymbol{\Phi}}_{\boldsymbol{\lambda'\theta}} & \tilde{\boldsymbol{\Phi}}_{\boldsymbol{\lambda'\lambda'}} & \tilde{\boldsymbol{\Phi}}_{\boldsymbol{\lambda'\lambda_\theta}} \\ \tilde{\boldsymbol{\Phi}}_{\boldsymbol{\lambda_\theta x'}} & \tilde{\boldsymbol{\Phi}}_{\boldsymbol{\lambda_\theta\theta}} & \tilde{\boldsymbol{\Phi}}_{\boldsymbol{\lambda_\theta\lambda'}} & \tilde{\boldsymbol{\Phi}}_{\boldsymbol{\lambda_\theta\lambda_\theta}} \end{bmatrix} \begin{bmatrix} \boldsymbol{\delta \mathbf{x}'_{\mathbf{ca}}} \\ \delta\theta_{ca} \\ \boldsymbol{\lambda'_{ca+}} \\ \lambda_{\theta_{ca+}} \end{bmatrix} \tag{33}$$

The STM and the co-state discontinuity are to reframe the state perturbation at TCA.

$$\delta\theta_{ca} = \nu\frac{M}{L} \tag{34a}$$

$$\boldsymbol{\delta \mathbf{x}'_{\mathbf{ca}}} = \nu\mathbf{B}^{-1}\mathbf{n} \tag{34b}$$

The two equations can be coupled to obtain:

$$\boldsymbol{\delta \mathbf{x}_{\mathbf{ca}}} = \nu\mathbf{h} \qquad \mathbf{h} = \begin{bmatrix} \mathbf{B}^{-1}\mathbf{n} \\ \frac{M}{L} \end{bmatrix} \tag{35}$$

$$\mathbf{x}(t_{ca}) = \mathbf{x}_{\mathbf{ref}}(t_{ca}) + \nu\mathbf{h} \tag{36}$$

Where:

$$\mathbf{B} = \tilde{\boldsymbol{\Phi}}_{\boldsymbol{x'x'}} + \tilde{\boldsymbol{\Phi}}_{\boldsymbol{x'\lambda'}}\mathbf{E} + \tilde{\boldsymbol{\Phi}}_{\boldsymbol{x'\lambda_\theta}}\mathbf{g} \qquad \mathbf{d} = \tilde{\boldsymbol{\Phi}}_{\boldsymbol{x'\theta}} + \tilde{\boldsymbol{\Phi}}_{\boldsymbol{x'\lambda'}}\mathbf{w} + P\tilde{\boldsymbol{\Phi}}_{\boldsymbol{x'\lambda_\theta}} \tag{37a}$$

$$M = \tilde{\boldsymbol{\Phi}}_{\boldsymbol{\lambda_\theta\lambda'}}\boldsymbol{\varphi'} + \tilde{\boldsymbol{\Phi}}_{\boldsymbol{\lambda_\theta\lambda_\theta}}\varphi_\theta - \tilde{\mathbf{b}}\left[\mathbf{B}^{-1}\left(\tilde{\boldsymbol{\Phi}}_{\boldsymbol{x'\lambda'}}\boldsymbol{\varphi'} + \tilde{\boldsymbol{\Phi}}_{\boldsymbol{x'\lambda_\theta}}\varphi_\theta\right)\right] \tag{37b}$$

$$L = \tilde{D} - \tilde{\mathbf{b}}(\mathbf{B}^{-1}\mathbf{d}) \tag{37c}$$

$$\tilde{\mathbf{b}} = \tilde{\boldsymbol{\Phi}}_{\boldsymbol{\lambda_\theta x'}} + \tilde{\boldsymbol{\Phi}}_{\boldsymbol{\lambda_\theta\lambda'}}\mathbf{E} + \tilde{\boldsymbol{\Phi}}_{\boldsymbol{\lambda_\theta\lambda_\theta}}\mathbf{g} \qquad \tilde{D} = \tilde{\boldsymbol{\Phi}}_{\boldsymbol{\lambda_\theta\theta}} + \tilde{\boldsymbol{\Phi}}_{\boldsymbol{\lambda_\theta\lambda'}}\mathbf{w} + P\tilde{\boldsymbol{\Phi}}_{\boldsymbol{\lambda_\theta\lambda_\theta}} \tag{37d}$$

$$\mathbf{n} = \tilde{\boldsymbol{\Phi}}_{\boldsymbol{x'\lambda'}}\boldsymbol{\varphi'} + \tilde{\boldsymbol{\Phi}}_{\boldsymbol{x'\lambda_\theta}}\varphi_\theta - \frac{M}{L}\mathbf{d} \tag{37e}$$

Defining $\boldsymbol{\rho}(\mathbf{x})$ as the function to pass from keplerian elements to position vector in ECI coordinates with a first-order Taylor approximation the constraint expression results:

$$\left[\boldsymbol{\rho}(\mathbf{x_{ca}}) - \mathbf{r_s}(t_{ca})\right]^T \mathbf{Q}\left[\boldsymbol{\rho}(\mathbf{x_{ca}}) - \mathbf{r_s}(t_{ca})\right] = \overline{SMD} \tag{38}$$

Where:

$$\mathbf{Q} = \mathbf{R_{2b}}^T\mathbf{C}^{-1}\mathbf{R_{2b}} \tag{39}$$

This equation has no closed-form solution. For this reason a first-order Taylor expansion of $\boldsymbol{\rho}(\mathbf{x})$ is used:

$$\boldsymbol{\rho}(\mathbf{x_{ca}}) \approx \mathbf{r_p}(t_{ca}) + \nu\mathbf{J}\mathbf{h} \tag{40}$$

with:

$$\mathbf{J} = \left.\frac{\partial\boldsymbol{\rho}(\mathbf{x})}{\partial\mathbf{x}}\right|_{\mathbf{x_{ref}}} \tag{41}$$

The polynomial in ν is then:

$$\left[\mathbf{r_p}(t_{ca}) + \nu\mathbf{J}\mathbf{h} - \mathbf{r_s}(t_{ca})\right]^T \mathbf{Q}\left[\mathbf{r_p}(t_{ca}) + \nu\mathbf{J}\mathbf{h} - \mathbf{r_s}(t_{ca})\right] = \overline{SMD} \tag{42}$$

RESULTS

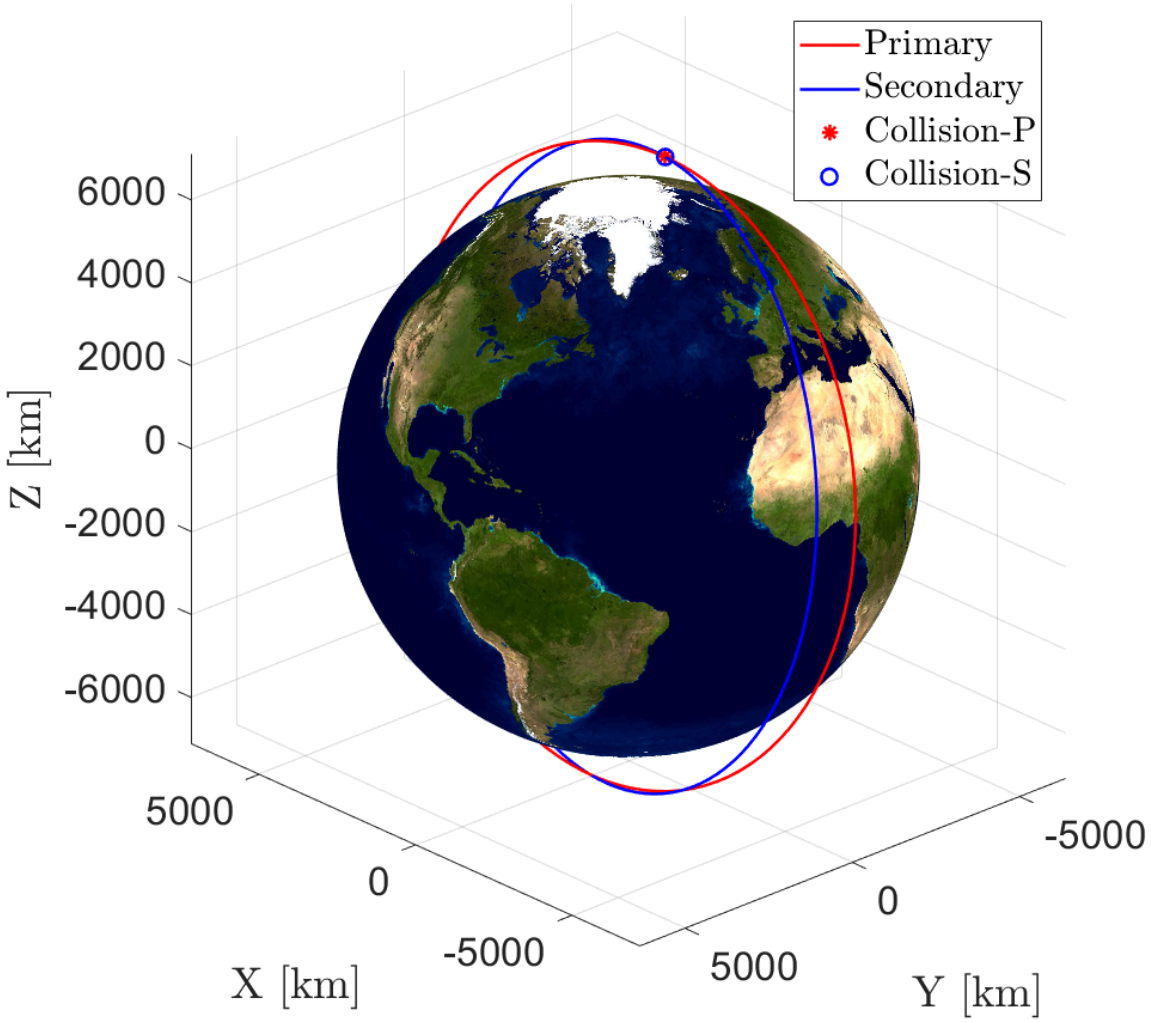

Figure 2: Conjunction test case.

The methods presented so far are applied to a test case extracted from,[11] a database of 2,170 conjunction cases taken from the ESA Collision Avoidance Challenge.[12] A representation of the collision can be found in Figure 2. Table 1 reports the position and velocity vectors of the primary and secondary spacecraft at the conjunction in ECI frame, the PoC, the SMD and the miss distance d. The combined cross-sectional radius of the spacecraft is $s_A = 29.7$ m. The Keplerian elements of the two orbits are computed and displayed in Table 2.

Table 1: Test case conjunction data.

$\vec{r}_p$[km]	[2.3305, -1103.7, 7105.9]$^\top$
$\vec{r}_s$[km]	[2.3335, -1103.7, 7105.9]$^\top$
$\vec{v}_p$ [km/s]	[-7.4429, -6.1373e-04, 3.9514e-03]$^\top$
$\vec{v}_s$ [km/s]	[7.3537, -1.1428, -0.19825]$^\top$
PoC	1.3604e-01
SMD	0.87166
d [km]	0.0432

Table 2: Test case orbital elements, in order: semi-major axis, eccentricity, inclination, Right Ascension of the Ascending Node (RAAN), the argument of the periapsis, true anomaly.

	a	e	i	Ω	ω	θ
O_p	7186.7 km	0.00064	98.83 °	0 °	289.38 °	160.60 °
O_s	7190.2 km	0.0024	81.28 °	170.93 °	184.41 °	266.99 °

The position covariance matrices of the two satellites, expressed in their respective ECI reference frame, are:

$$\vec{C}_p = \begin{bmatrix} 0.9317 & -2.6234 & 0.2360 \\ -2.6234 & 1778.0 & -0.9331 \\ 0.2360 & -0.9331 & 0.1917 \end{bmatrix} \cdot 10^{-4}\ \mathrm{km}^2 \tag{43}$$

$$\vec{C}_s = \begin{bmatrix} 6.3466 & -19.6229 & 0.7077 \\ -19.6229 & 0.0820 & 11.3982 \\ 0.7077 & 11.3982 & 2.5103 \end{bmatrix} \cdot 10^{-4}\ \mathrm{km}^2 \tag{44}$$

The corresponding combined covariance matrix in B-plane coordinates is:

$$\vec{C} = \begin{bmatrix} 7.21756 & -0.7580 \\ -0.7580 & 51.9201 \end{bmatrix} \cdot 10^{-4}\ \mathrm{km}^2 \tag{45}$$

In the following section, the methods are compared using a dynamical model which only considers Keplerian motion, as expressed in Eq. 12.
All the simulations presented in this dissertation are run with an Intel(R) Core(TM) i7-10700 CPU processor with 16 GB of Ram Memory.

The results reported in this section with a collision probability $PoC = 10^{-6}$ leads to a threshold of $SMD = 26.9016$.

Point-to-Point with intermediate CAM constraint

In Fig. 3, the object TCA always sticks to the iso-probability ellipse. The transfer time spans between 2 and 4 periods. In the plots shown hereafter, t_{back} (from one to two orbital periods) embodies the time range between the initial maneuvering point to TCA and t_{after} (from one to two orbital periods as well) from TCA to the reentry time. The same plot for t_{back} is not displayed inasmuch as the b-plane points would be the same apart from colouring.

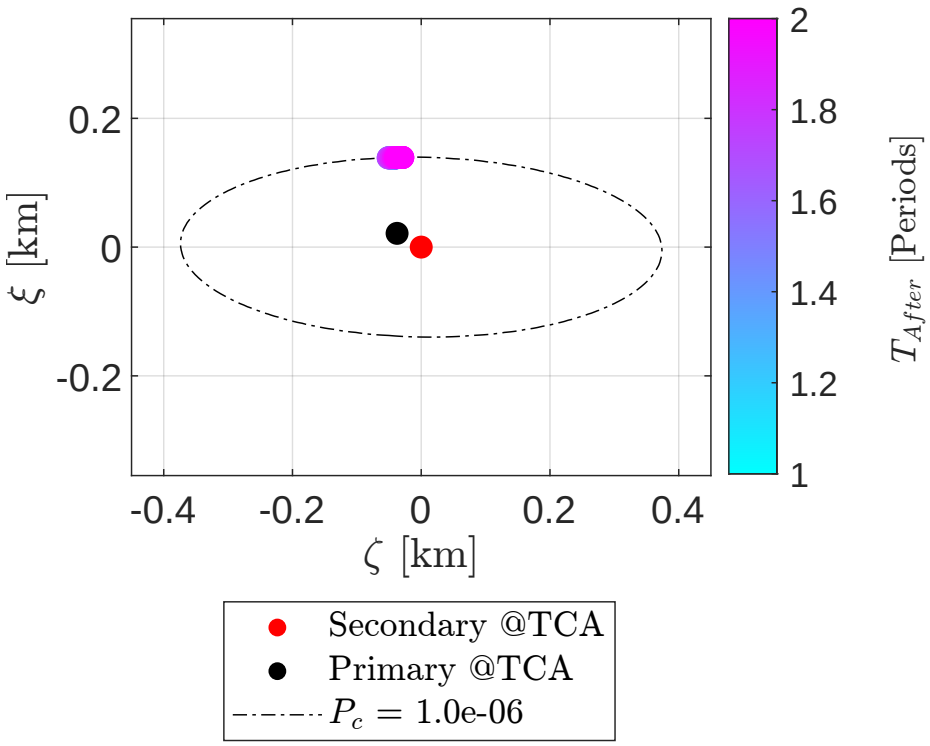

Figure 3: B-plane representation for the EOP PTP solution.

Looking at Fig. 4, the Δv spent is reported as a surf plot with a grid of 15 by 15 elements. Planning a CAM in advance (for $t_{back} \approx 2$ and $t_{after} \approx 2$) does not imply a Δv reduction because the primary is constrained to land on a target point potentially not optimal for that time range.

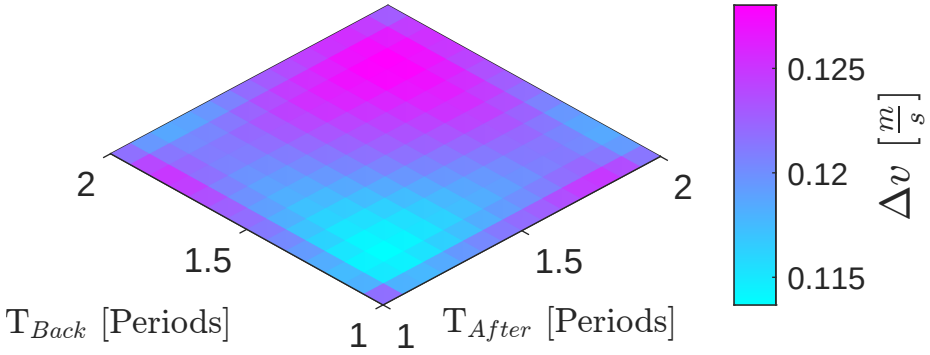

Figure 4: Δv surface for the EOP PTP solution.

When it comes to the acceleration components in the RTN frame, Fig. 5 suggests that an in-plane maneuver works best. Indeed, in the literature, CAM alone is optimally executed with tangential and radial firings. On top, the costate discontinuity condition at TCA implies an abrupt change in the component-wise slope.

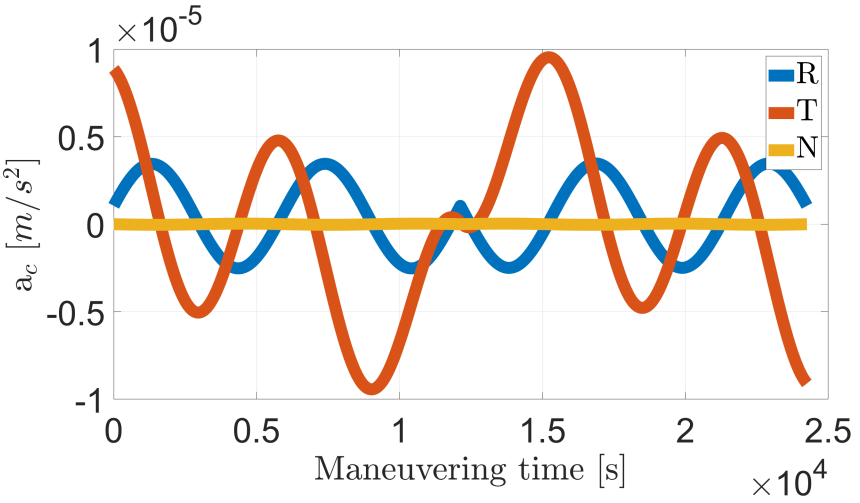

Figure 5: PTP Acceleration components in RTN for $T_{back} = 2\ periods$ and $T_{after} = 2\ periods$

Finally, Fig. 6 evaluates the terminal position error. Varying t_{back} or t_{after} does not affect the solution's accuracy. The offset is just decimeters, well below the average spacecraft position uncertainty.

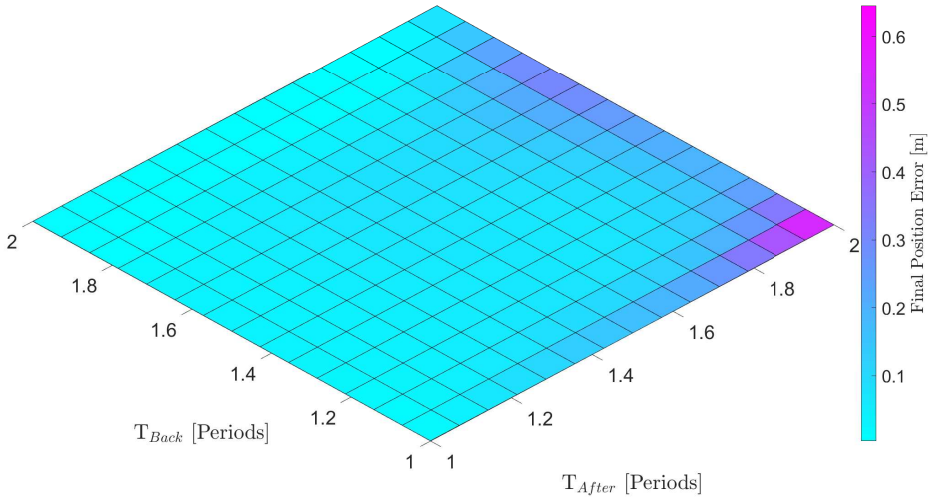

Figure 6: Final position error for the PTP strategy

The computational time is reported for PTP in Fig. 7. It encompasses the STMs integration (the most expensive operation) and the procedure to get and solve the polynomial spanning across all the roots. The numerical effort of the analytic solution is strongly influenced by the propagation time, as seen with an upward trend for higher t_{back} and t_{after}. Given the attained performance, such a solution strategy may apply to large-scale simulations or may provide a good guess for advanced numerical methods including mission constraints. The pipeline has been developed in Matlab; a compiled C++ version would certainly lessen this figure of merit.

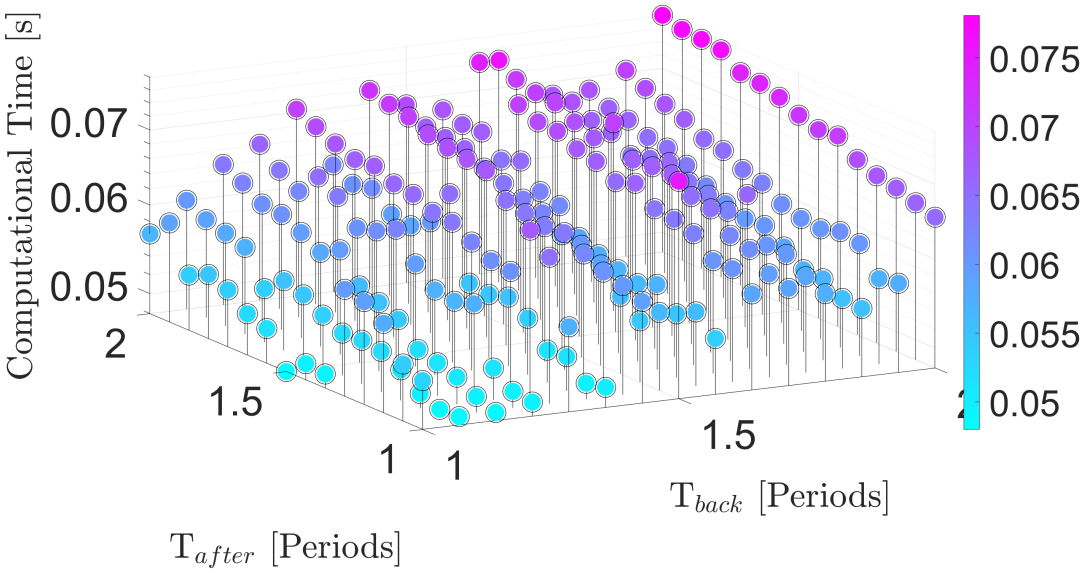

Figure 7: EO PTP computational time

Point-to-Orbit with intermediate CAM constraint

Position-wise on the Bplane (see Fig. 8), the singled-out points slightly move leftward compared to Fig. 3 still attaining the same accuracy level.

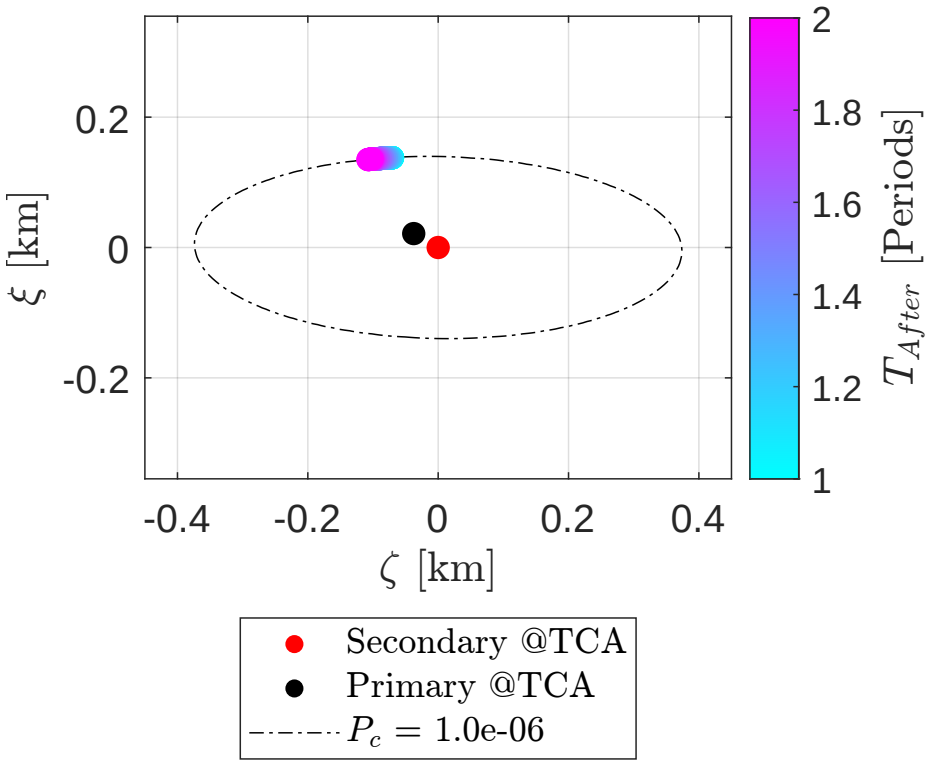

Figure 8: B-plane representation for the EOP PTO solution.

Moving on to the maneuver cost, letting the true anomaly free makes the Δv almost halve for some combinations of t_{back} and t_{after} if likened to Fig. 4.

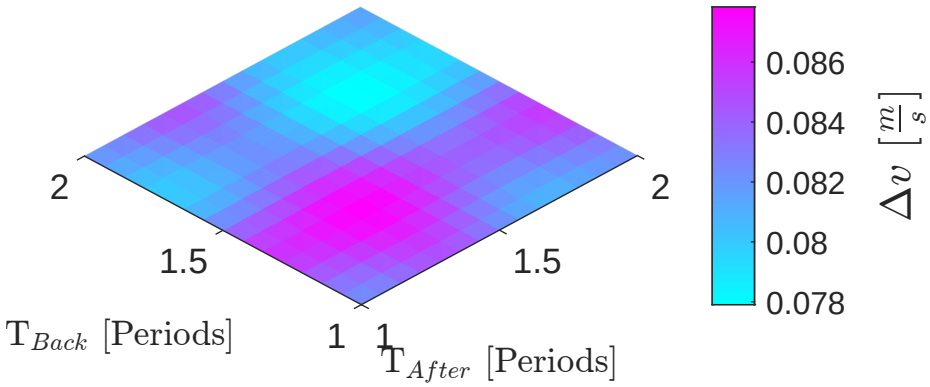

Figure 9: Δv surface for the EOP PTO solution.

Figure 10, with the acceleration magnitude profile, corroborates Δv efficiency of the PTO solu-

tion: on average, it has a lower mean acceleration level.

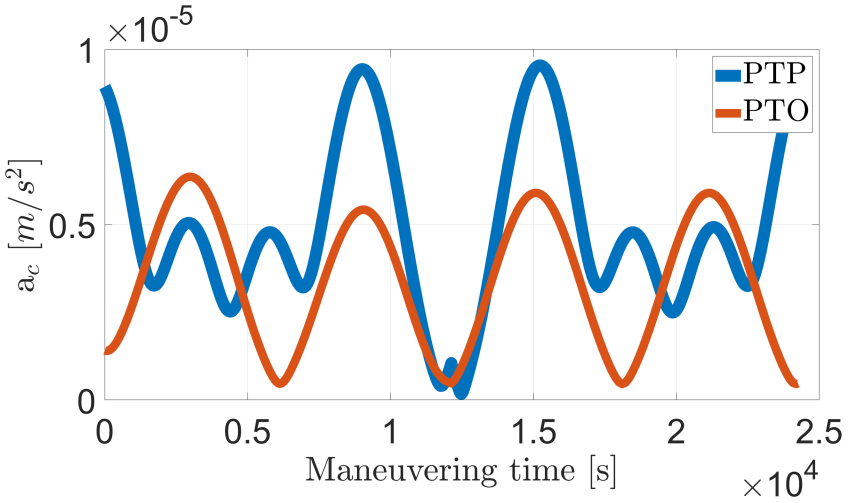

Figure 10: Acceleration magnitude comparison between PTP and PTO for $T_{back} = 2\ periods$ and $T_{after} = 2\ periods$

The PTO strategy confirm the trend in Fig. 11 that an in-plane maneuver is beneficial for fuel savings.

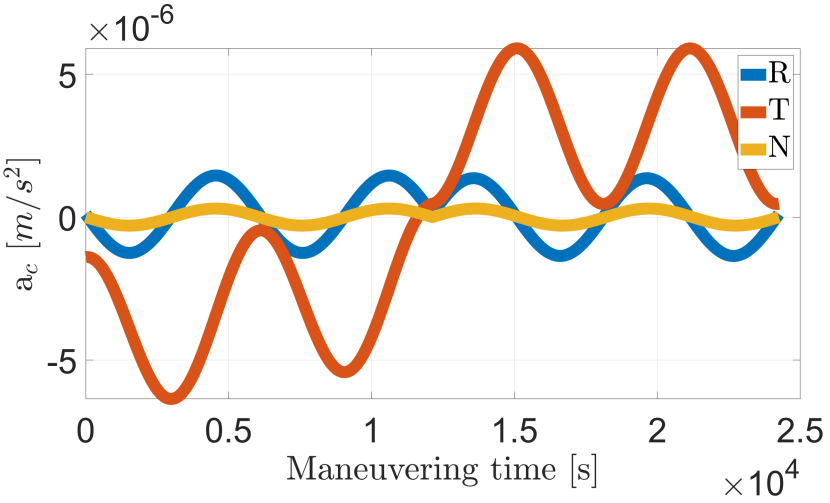

Figure 11: PTO Acceleration components in RTN for $T_{back} = 2\ periods$ and $T_{after} = 2\ periods$

The PTO case consumes less for the same PTP time span at the expense of a delayed reentry in true anomaly terms. As can be seen in Fig. 12 the gap is almost negligible unless having constraints on the spacecraft return point.

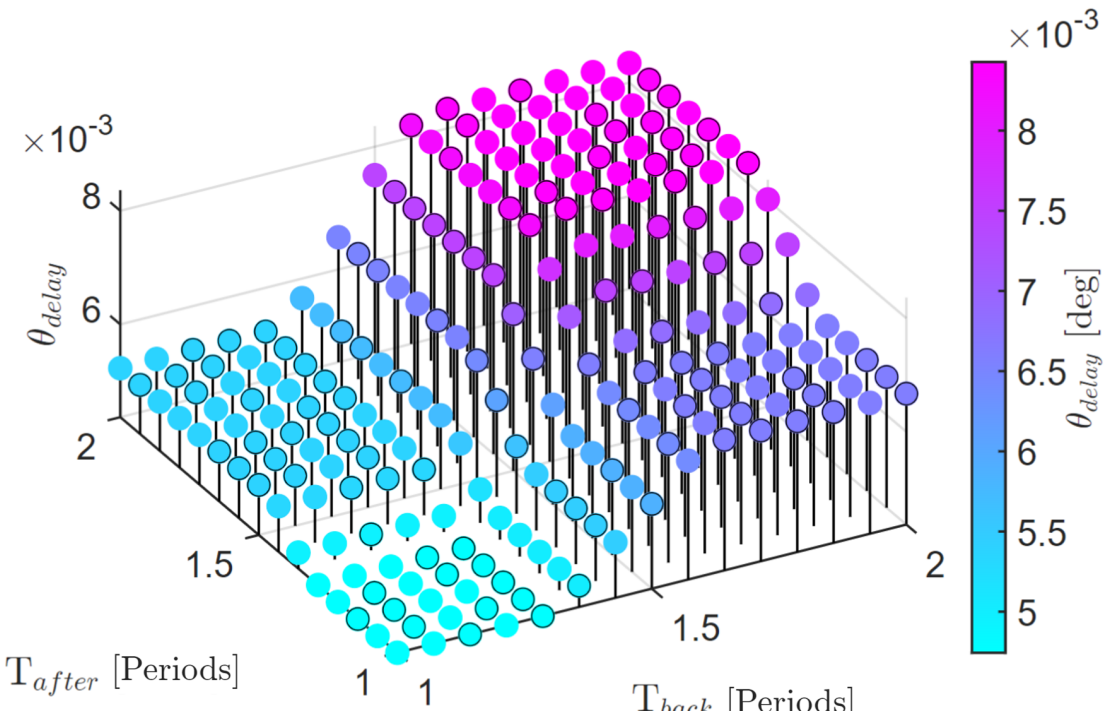

Figure 12: θ_{delay} difference.

The computational burden for PTO is shown in Fig. 13. It shares similar considerations to the PTP counterpart in terms of overall achieved performance.

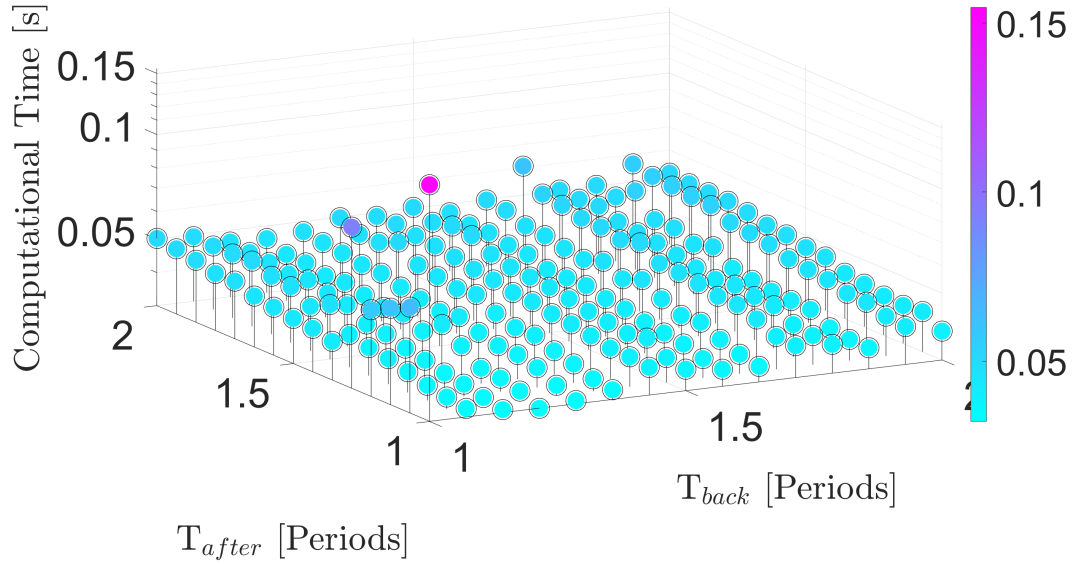

Figure 13: PTO computational time

CONCLUSIONS

In this work, pioneering CAM strategies with adjoined return to initial spacecraft orbit present a step forward for in-orbit maneuver planning. Comparing the equation of motions of the ECI formalism with the Gauss interplanetary ones, it is noticeable how playing with the true anomaly can almost halve the Δv for the same firing time. The output control is computed in a fraction of a second, making the algorithm look even brighter for future onboard implementation. As a next step, the Energy Optimal Control Problem (EOCP) guess can be further processed to design more operative scenarios where satellites follow typical bang-bang structures that are easier to execute and grant an extra fuel mass savings.

REFERENCES

[1] ESA, "SSA Programme overview," 2022.

[2] J. A. Reiter and D. B. Spencer, "Solutions to rapid collision-avoidance maneuvers constrained by mission performance requirements," *Journal of Spacecraft and Rockets*, Vol. 55, No. 4, 2018, pp. 1040–1048.

[3] A. De Vittori, M. Palermo, P. Di Lizia, and R. Armellin, "Low-Thrust Collision Avoidance Maneuver Optimization," *Journal of Guidance, Control, and Dynamics*, Vol. 45, 08 2022, pp. 1–15, 10.2514/1.G006630.

[4] J. Gonzalo Gomez, C. Colombo, and P. Di Lizia, "A semi-analytical approach to low-thrust collision avoidance manoeuvre design," *70th International Astronautical Congress (IAC 2019)*, 2019, pp. 1–9.

[5] J. Hernando-Ayuso and C. Bombardelli, "Low-Thrust Collision Avoidance in Circular Orbits," *Journal of Guidance, Control, and Dynamics*, 2021, pp. 1–13.

[6] Martínez Chamarro, C. Belmonte Hernandez, and R. Armellin, "Design of Collision Avoidance Maneuvers using Optimal Control Theory and Convex Optimization," *31st Space Flight Mechanics Meeting*, 2021.

[7] S.-C. Lee, H.-D. Kim, and J. Suk, "Collision Avoidance Maneuver Planning Using GA for LEO and GEO Satellite Maintained in Keeping Area," *International Journal of Aeronautical and Space Sciences*, Vol. 13, 2012, pp. 474–483.

[8] A. Cantoni, "Numerically Efficient Methods ForLow-Thrust Collision Avoidance Manoeuvres Design in GEO Regime," *73rd International Astronautical Congress (IAC),Paris, France, 18-22 September 2022*, 09 2022, pp. 1–12.

[9] C. Bombardelli, "Analytical formulation of impulsive collision avoidance dynamics," *Celestial Mechanics and Dynamical Astronomy*, Vol. 118, 11 2013, pp. 77–, 10.1007/s10569-013-9526-3.

[10] J. Hernando-Ayuso and C. Bombardelli, "Low-Thrust Collision Avoidance in Circular Orbits," *Journal of Guidance, Control, and Dynamics*, Vol. 44, May 2021, pp. 983–995, 10.2514/1.g005547.

[11] R. Armellin, "Github, `https://github.com/arma1978/conjunction/`,"

[12] T. Uriot, D. Izzo, L. Simoes, R. Abay, N. Einecke, S. Rebhan, J. Martinez-Heras, F. Letizia, J. Siminski, and K. Merz, "Spacecraft Collision Avoidance Challenge: design and results of a machine learning competition," *arXiv preprint arXiv:2008.03069*, 2020.